A wavelet analysis of low-wind-speed submeso motions in a nocturnal boundary layer

RMetS
Royal Meteorological Society

A wavelet analysis of low-wind-speed submeso motions in a nocturnal boundary layer

D. Cava,[a]* L. Mortarini,[b] U. Giostra,[c,d] R. Richiardone[e] and D. Anfossi[b]

[a]*National Research Council, Institute of Atmospheric Sciences and Climate, Lecce, Italy*
[b]*National Research Council, Institute of Atmospheric Sciences and Climate,Turin, Italy*
[c]*Department of Pure and Applied Sciences (DiSPeA), Università degli Studi di Urbino 'Carlo Bo', Italy*
[d]*National Inter-University Consortium for Physics of the Atmosphere and Hydrosphere (CINFAI), Rome, Italy*
[e]*Dipartimento di Fisica, Università di Torino, Italy*

*Correspondence to: D. Cava, National Research Council-Institute of Atmospheric Sciences and Climate – Lecce s.p. Lecce-Monteroni km 1.2, 73100 Lecce, Italy. E-mail: d.cava@le.isac.cnr.it

In low-wind regimes (wind speed less than 1.5 m s^{-1}) the nocturnal boundary layer is still inadequately understood. In such conditions, turbulence is weak and often intermittent, whereas dynamics and total fluxes are often driven by submeso motions. As a consequence, the momentum, mass and energy transfers are poorly represented by dispersion models. In low-wind conditions, an important fraction of submeso motions is represented by meandering modes, which can be detected through the Eulerian autocorrelation functions of horizontal wind components and temperature. Such an approach has been proven to be reliable. However, a deeper insight could be useful for understanding the phenomenon, especially when complex or multiple mesoscale motions simultaneously develop. In this work, Eulerian autocorrelation functions and the Morlet continuous wavelet transform were used to investigate an 8 h nocturnal period characterized by the coexistence of horizontal meandering and vertical oscillations, rarely observed elsewhere. This 'nice' episode represents a good case-study to compare the two used methodologies and to investigate the phenomenology of the two submeso phenomena simultaneously occurring in a low-wind-speed regime. The two methodologies identified the same time-scale for the detected meandering structures over the whole period. Moreover, the wavelet analysis: (i) was able to discriminate horizontal meandering and gravity waves, which simultaneously developed in the second part of the analysed period; (ii) showed that, in the investigated case, the horizontal meandering was not triggered by gravity waves which appeared later in the night; (iii) highlighted how both gravity waves and meandering can contribute to an increase of the vertical turbulent energy and fluxes, confirming the crucial role of submeso structures in the turbulence production during low-wind regimes in stable conditions.

Key Words: meandering; gravity waves; low-wind conditions; atmospheric turbulence; stable boundary layer; wavelet analysis; Eulerian autocorrelation functions

Received 15 June 2016; Revised 13 October 2016; Accepted 22 October 2016; Published online in Wiley Online Library

1. Introduction

The dynamics of the stable boundary layer (SBL) has been investigated in numerous studies over the past decades. Significant progress has been made in understanding the main characteristics in the stable regime where the turbulence is fairly continuous in both time and space and decreases with height up to the top of a quite well-defined boundary layer. In such conditions the turbulent structure can be described by similarity theory and parametrizations (Wyngaard, 2010).

On the other hand, the main features of the SBL still remain poorly understood in low-wind regimes (wind speed less than 1.5 m s^{-1}) (Anfossi *et al.*, 2005) because of the complex interaction of multiple-scale processes (Mahrt, 2014). In these conditions it is difficult to identify a classical structure of the boundary layer as the turbulence becomes extremely weak and strongly intermittent. Turbulent statistics are often influenced by irregular small-scale eddies that do not directly interact with the ground (z-less stratifications) (Nieuwstadt, 1984; Dias *et al.*, 1995; Mahrt, 1999). Moreover, turbulent transport appears also driven by large downward bursting related to intermittent short-term wind accelerations above a height-dependent threshold value (Mahrt, 2011; Sun *et al.*, 2012). These infrequent mixing events account for much of the total flux

and are modulated by various non-turbulent submeso motions, on scales from metres to a few kilometres which can produce significant flow non-stationarity (Mahrt, 2010; Vercauteren *et al.*, 2016).

Typical submeso motions include gravity waves (GWs; De Baas and Driedonks, 1985; Chimonas, 2002; Nappo, 2002), microfronts, two-dimensional modes (like meandering motions or pancakes vortices; Anfossi *et al.*, 2005; Mahrt, 2007; Mortarini *et al.*, 2013, 2016a), drainage flows (Doran and Horst, 1981), density currents and solitary waves (Sun *et al.*, 2004; Terradellas *et al.*, 2005) and other complex structures. The dynamics of such motions and their influence on the generation of intermittent mixing events in the SBL are poorly understood and, as a consequence, usually not well represented in the dispersion models which often fail in estimating pollutant concentrations in low-wind-speed conditions (Gupta *et al.*, 1997; Anfossi *et al.*, 2006; Vickers *et al.*, 2008; Mahrt and Mills, 2009; Belušic and Güttler, 2010).

Wave-like structures are fundamental features of the SBL and their influence on the transport of momentum, mass and energy throughout the atmosphere has been the most extensively studied among all other submeso motions (Rees *et al.*, 2000; Nappo, 2002; Cava *et al.*, 2004, 2015; Viana *et al.*, 2010; Durden *et al.*, 2013; Sorbjan and Czerwinska, 2013; Nappo *et al.*, 2014). Nonetheless, the description of GW dynamics and the parametrization of turbulence–wave interaction remain an open question.

An important fraction of submeso motions is represented by meandering modes which, as well as GWs, can modulate the intermittent turbulent production in the SBL in low-wind conditions. Moreover they can cause large horizontal dispersion usually not captured in dispersion models (Sharan *et al.*, 2003; Anfossi *et al.*, 2006) in the absence of a proper physical understanding of the meandering dynamics.

Meandering does not have a precise definition; it generally refers to large horizontal oscillations of the wind direction due to a complex mix of motions on scales between the main turbulent eddies and the smallest mesoscale motions (Joffre and Laurila, 1988; Belušić and Mahrt, 2008; Vickers *et al.*, 2008). There is not a general consensus on the physical causes responsible for the wind meandering during low-wind-speed conditions. They include surface pressure perturbations induced by mesoscale motions, internal GWs, quasi-2D pancake motions, pulsating drainage flows, solitons, and vortices with either a horizontal or a vertical axis (Mahrt, 2007). Although meandering has also been observed at low wind speeds in neutral and unstable conditions (Sharan *et al.,* 2003; Anfossi *et al.*, 2005; Mahrt, 2011; Mortarini *et al.*, 2013, 2016a, 2016b), in most studies stable stratification is considered a necessary condition for observing meandering flows (Mahrt, 2014 gives a review). Starting from the works of Oettl *et al.* (2001) and Anfossi *et al.* (2005) in low-wind-speed conditions, Mortarini *et al.* (2016a, 2016b) defined meandering as a non-turbulent oscillation of the temperature and horizontal wind velocity components and characterized it through the evaluation on hourly datasets of the Eulerian autocorrelation function (EAF). By fitting the temperature and horizontal wind velocity component EAFs with an oscillating function (Frenkiel, 1953; Murgatroyd, 1969), it is possible to determine a loop parameter that identifies the ratio of time-scales of small-scale and large-scale oscillatory motions (Anfossi *et al.*, 2005; Mortarini *et al.*, 2013) and identifies meandering and non-meandering cases (Mortarini *et al.*, 2016b). The EAFs fit also allows the estimation of the meandering time-scale, i.e. of the time-scale of the low-frequency submeso motions associated with the meandering phenomenon.

In this work we present the analysis of wind, temperature and pressure fluctuations collected in a low-wind stably stratified night observed during the Urban Turbulent Project in Turin, Italy (UTP;Trini Castelli *et al.*, 2014). This episode was chosen for the simultaneous presence of horizontal wind meandering and vertical submeso oscillations rarely observed in previous studies (Anfossi *et al.*, 2005; Mortarini *et al.*, 2016a).

An original approach is proposed here to estimate the meandering time-scales of the wind velocity and temperature using two complementary methodologies. First, we used the Mortarini *et al.* (2016a) method based on the EAFs and then we compared these results with a wavelet analysis. The continuous wavelet transform based on the Morlet basis was used to detect and characterize the time-scale of the wavelike oscillations both in the wind velocity and in the temperature signals and their connections with pressure fluctuations. Moreover, cross-wavelet spectra were used to identify the nature of the wavy patterns in order to discriminate the presence of GWs. The wavelet analysis corroborated the results obtained with the EAFs and opened new promising perspectives for the study of the meandering phenomenon.

2. Experimental site and measurements

The UTP experiment (Mortarini *et al.*, 2013; Trini Castelli *et al.*, 2014) was held in Turin (about 900 000 inhabitants), located at the western edge of the Po Valley at 220 m amsl (above mean sea level). Turin city covers an area of about 130 km^2 and the eastern sector lies at the foot of a hill range (maximum altitude of about 700 m amsl); the other three sectors are surrounded by the Alps (with crest line at about 100 km distant), and the Apennines to the south. The UTP station (45.018°N, 7.643°E) was a suburban meteorological station located in an area on the southern outskirts of the town on grassy, flat terrain surrounded by buildings and some open-field plots. The distance of tallest buildings (about 30 m high) from the measuring site was about 150 m in the north to northeast direction, while in the other directions the closest buildings, characterized by heights ranging from 4 to 18 m, were at about 70–90 m distance. Therefore, the measurements were taken in a complex and mixed geometry and were not representative of a typical street-canyon configuration or dense urban canopy.

A ground-based 25 m mast, equipped with horizontal booms pointing west and east at 5, 9 and 25 m heights, was located at the centre of the station; there were also two booms pointing north and south installed at 25 m height. There were three anemometers, recording at 20 Hz the three wind velocity components (u, v, w, respectively the longitudinal, lateral and vertical component) and the sonic temperature (θ): two Gill Solent 1012R2 placed at 5 and 9 m, and a Gill Solent 1012R2A at 25 m. However, during the examined night the 25 m anemometer was out of operation. Near the ground a differential microbarometer (Richiardone, 1993) measured the atmospheric pressure fluctuations (Δp). The instrument resolution of 0.2 Pa allowed an optimal accuracy since the typical amplitude of pressure fluctuations due to GWs was of the order of 10 Pa.

3. Methods of analysis

In this section the methodologies applied in the data analysis are briefly summarized.

3.1. Eulerian autocorrelation function

Different authors (Oettl *et al.*, 2001; Anfossi *et al.*, 2005) found and others (Steeneveld and Holtslag, 2011; Luhar, 2012) confirmed that the meandering phenomenon can be well represented in a mathematical framework by an EAF with a distinctive negative lobe.

For a generic stationary process χ, the EAF, $R_\chi(\tau)$, is defined as

$$R_\chi(\tau) = \frac{\langle \chi(t+\tau)\,\chi(\tau)\rangle}{\sigma_\chi^2}. \quad (1)$$

Both numerical and analytical approaches (Oettl *et al.*, 2005; Goulart *et al.*, 2007) showed that, when the wind speed decreases

below a threshold value (around 1.5 m s^{-1}), the wind velocity EAF assumes the form (Frenkiel, 1953; Murgatroyd, 1969):

$$R(\tau) = e^{-p\tau} cos(q\tau), \tag{2}$$

where the parameter p is connected with the turbulence time-scale, and the parameter q is associated with the meandering characteristics (Mortarini *et al.*, 2013). Mortarini *et al.* (2016a) showed that in low-wind-speed conditions the temperature also frequently exhibits the oscillating behaviour described by Eq. (2).

Through p and q it is possible to define the loop parameter, $m = q/p$, and the meandering time-scale

$$T_* = \frac{2\pi}{q}. \tag{3}$$

The loop parameter describes the ratio of the time-scales of the submeso meandering motions associated with q and the small-scale turbulent motions associated with p. High values of m are associated with a meandering phenomenon occurring on scales larger than the turbulent time-scale. Low values of m are associated with a turbulent time-scale larger than the identified meandering time-scale and the meandering phenomenon is therefore deemed negligible. Mortarini *et al.* (2016a, 2016b) use the loop parameter to discriminate between meandering and not-meandering cases. Following their methodology in this work we identified meandering episodes when

$$\begin{cases} \overline{u} \leq 1.5 \text{ m s}^{-1} \\ m_{u,v,\theta} \geq 1 \end{cases}, \tag{4}$$

where $\bar{u}$ is the mean wind speed.

The meandering time T_* identifies the time-scale of the submeso processes associated with the meandering phenomenon. However, the estimation of T_* may depends on the duration of the time series used to evaluate the EAF. In fact, Mortarini *et al.* (2013) noticed that, when fitting the autocorrelation function with Eq. (2) to evaluate p and q, the maximum allowed value for q is related to the length of the sampling time.

3.2. Wavelet analysis

Wavelet analysis is a mathematical tool frequently used in geophysical studies for its versatile applicability. Localization properties of the wavelet transform are especially advantageous for decomposing a signal into time and frequency components, and for determining its dominant modes and their time evolution (Daubechies, 1992; Farge, 1992).

Wavelets have been efficiently used in atmospheric boundary-layer studies for investigating the intermittent periodicities and the non-stationary character of atmospheric turbulence and its interaction with larger structures such as GWs, meandering or drainage flows (Howell and Mahrt, 1997; Katul and Vidakovic, 1998; Rees *et al.*, 2001; Cava *et al.*, 2005, 2015; Viana *et al.*, 2010; Durden *et al.*, 2013; Sun *et al.*, 2015).

Detailed tutorial papers on wavelet theory and applications to the analysis of geophysical data have been published in the literature (Kumar and Foufoula-Georgiou, 1997; Torrence and Compo, 1998). In the following only a brief summary of the methodology used in this study will be included.

The wavelet transform $Wf(\lambda,t)$ of a function $f(t)$ with finite energy is defined as the integral transform with a family of functions $\psi_{\lambda,t}(u) = \frac{1}{\sqrt{\lambda}}\psi\left(\frac{u-t}{\lambda}\right)$ and is given by:

$$Wf(\lambda,t) = \int_{-\infty}^{\infty} f(u) \quad \psi_{\lambda,t}(u)\mathrm{d}u, \tag{5}$$

where $\lambda(>0)$ is a scale parameter and t is a location parameter. Changing the value of λ has the effect of dilating or contracting the function ψ (called mother wavelet), i.e. of analysing the function $f(t)$ at different spatial scales; whereas changing t has the effect of analysing the function $f(t)$ around the point t.

In this work a continuous wavelet analysis was applied in order to investigate the characteristics of the submeso motions embedded in the analysed time series. The Morlet function has been chosen as mother wavelet for its high resolution in frequency space, well suited for the determination of the period of detected meandering or wavy events (Thomas and Foken, 2005).

The wavelet spectra

$$S = |Wf(\lambda,t)|^2 \tag{6}$$

provide an estimation of the time evolution of the energy of the analysed signals as a function of the resolved time-scales (or frequencies).

Moreover, the common variability in frequency and time of different signals (f, g) can be computed through the wavelet cross-spectrum $W_{f,g} = Wf(\lambda,t).^* Wg(\lambda,t)$; the cospectrum (Co), i.e. the real part of $W_{f,g}$, is proportional to the covariance between the two time series, whereas the quad-spectrum (Q), i.e. the complex part of $W_{f,g}$, represents the spectrum of the product of f and g shifted by 90°. Furthermore, it is possible to define the wavelet coherence spectrum $\left(Coh = \frac{(Co^2+Q^2)}{S_f S_g}\right)$, which reveals significant coherence between two signals even if the common power is low, and the wavelet phase spectrum $(\varphi = \tan^{-1}(Q/Co))$ which gives information about the phase difference between f and g (Grinsted *et al.*, 2004).

In particular, cross-spectral statistics can be used for the identification of GW events in the measured series. In fact, in the presence of linear waves, the lack of vertical diffusion produces fluctuations of vertical velocity and scalars 90° out of phase. Therefore, in the wave source region, the quad-spectrum is larger than the cospectrum, the phase spectrum assumes values close to ±90°, and the coherence spectrum is close to 1 (de Baas and Driedonks, 1985).

4. Results

In this work we analysed 8 h of data measured on 11 December 2007 between midnight and 0800 (local time, LT= UTC + 1) in stable conditions. Data consisted of sonic anemometer measurements (u, v, w, θ), collected at 5 m and 9 m, and of pressure fluctuations (Δp) measured by a differential microbarometer at ground level. The wind velocities were rotated using the triple rotation method (McMillen, 1988; Cassardo *et al.*, 1995; Cava *et al.*, 2001) and linear trends were removed.

Figure 1 displays the time series for the analysed variables. Even if the instantaneous wind velocity values can exceed 2.5 m s^{-1}, the mean speeds evaluated on hourly subsets (not shown) are never larger than 0.6 m s^{-1}, well below the threshold for a low-wind-speed regime. For the most part, the horizontal wind velocity components show marked oscillations between 0130 and 0700 LT, particularly evident in the v-component between 0300 and 0400 and in the u-component between 0430 and 0630 The w-component often exhibits an increase in fluctuations alongside the oscillations of the horizontal wind velocities. Similar patterns are also present in the temperature and the pressure fluctuation time series. In particular, between 0430 and 0600 LT, the pressure fluctuations show a very regular wavy pattern.

The oscillating behaviour of the time series was first studied by means of the EAFs. The dataset was divided into subsets of 1 h and for each hour the EAFs of the wind velocity components, and the temperature and the pressure fluctuations were evaluated. Then the Mortarini *et al.* (2016a) criterion (Eq. (4)) was used to identify meandering episodes. At 9 m, six of the eight analysed hours were found to exhibit a meandering behaviour; only the third and fifth hours did not satisfy Eq. (4) because of an unclear oscillating behaviour of the temperature EAF (Figures S1(a) and (b)).

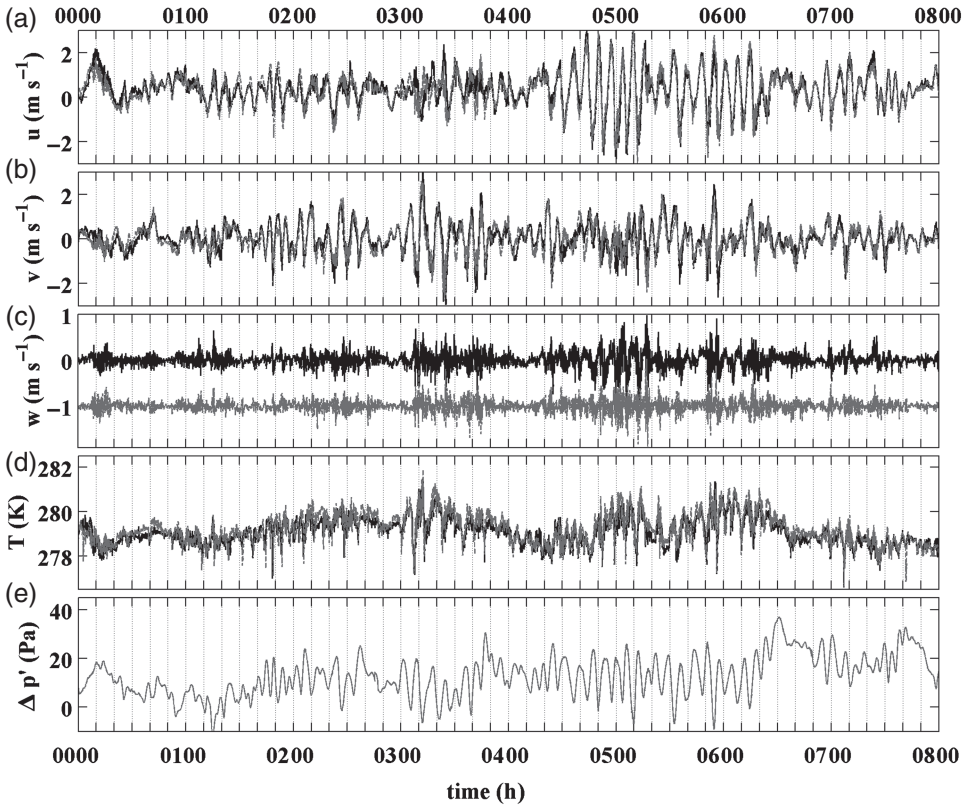

Figure 1. Time series of (a) longitudinal, (b) lateral and (c) vertical wind velocity components, (d) sonic temperature collected at 9 m (black lines) and 5 m (grey lines), and (e) pressure fluctuations collected at ground level on 11 December 2007. For a better comparison, the wind vertical component at 5 m has been artificially shifted.

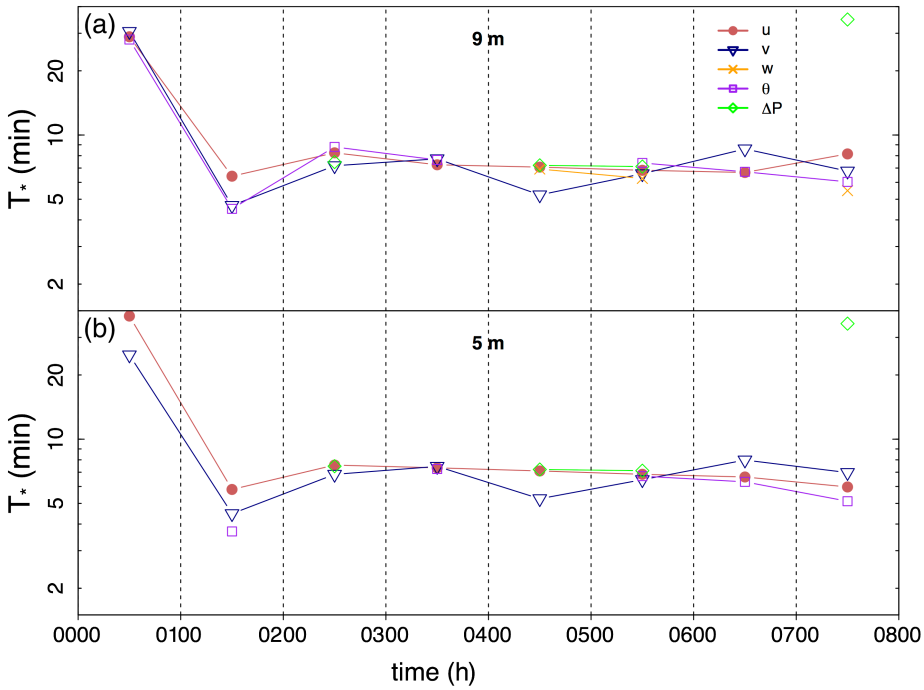

Figure 2. Meandering time-scales (Eq. (3)) for the analysed variables collected at (a) 9 m and (b) 5 m. Only the values where the EAFs fit Eq. (2) are shown in the plots.

Figure 2 shows the meandering time-scales (Eq. (3)) for the analysed variables; $T_{*\Delta p}$ is shown in both panels for the sake of comparison. It is worth stressing that Figure 2 shows the meandering time-scales evaluated using Eq. (3) every time the EAF function of a single quantity (u, v, w, θ, ΔP) fits Eq. (2) and not only when the meandering condition (Eq. (4)) is satisfied. In the first hour the oscillating behaviour is evident in the u and v velocity components at both the measurement levels and in the temperature at 9 m, but the meandering time-scale values are different from the ones evaluated for the following hours. From the second hour until the end of the analysed period, the T_* for all the variables converge to a value of about 8 min. For the pressure fluctuations, the EAFs identify a meandering time-scale on the third, fifth and sixth hours, while for the w-velocity component the EAFs recognise an oscillating behaviour in the fifth and sixth hours.

This procedure allows the detection of the meandering phenomenon when there is a clear separation between turbulent and submeso motions. However, as it can be seen in the temperature EAFs of the third and fifth hours at 9 m (Figures S1(a) and (b)), when more wave modes are simultaneously present, the

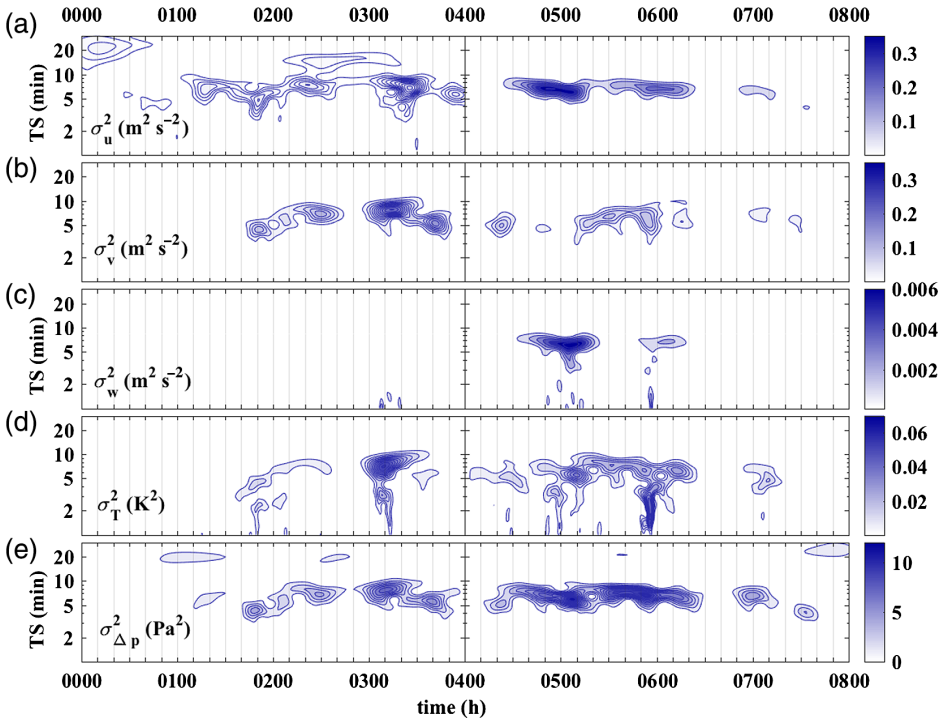

Figure 3. Time evolution in the submeso time-scale (TS) range of wavelet energy spectra of (a) longitudinal, (b) lateral and (c) vertical wind velocity components, (d) temperature collected at 9 m, and (e) pressure fluctuations collected at ground level on 11 December 2007.

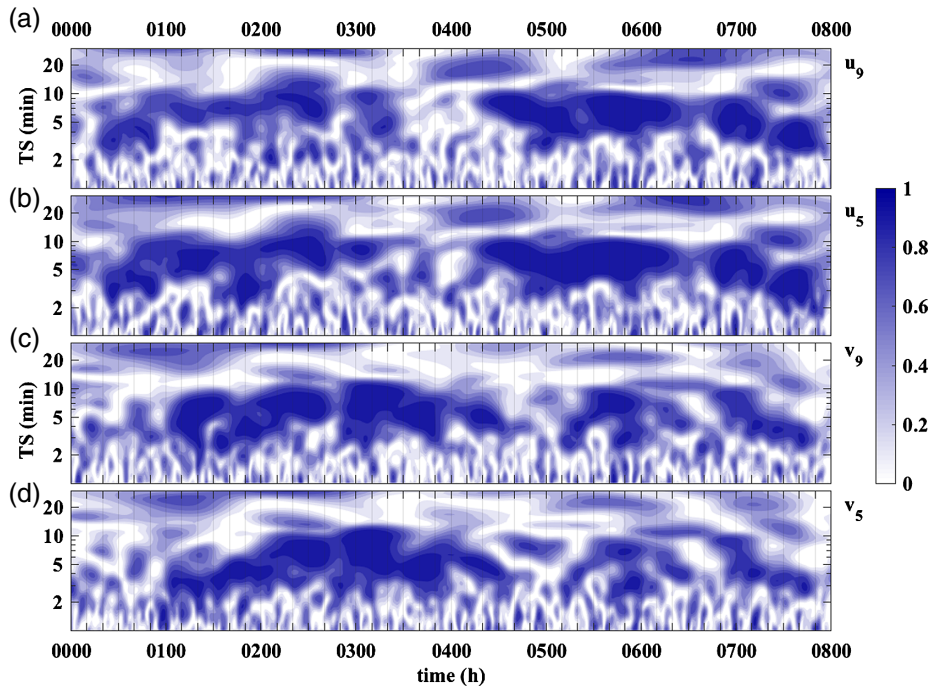

Figure 4. Time evolution in the submeso time-scale (TS) range of wavelet coherency spectra for the cross-correlation between pressure fluctuations and longitudinal wind component at (a) 9 m (u_9) and (b) 5 m (u_5) and lateral wind components at (c) 9 m (v_9) and (d) 5 m (v_5) collected on 11 December 2007.

fitting procedure fails. Moreover, the EAFs procedure does not permit determination of the nature of the oscillating structures and does not allow us to state if the differences in the T_* estimation among different variables are significant.

For these reasons a wavelet analysis may help in characterizing the wave phenomena and in isolating the turbulent components from submeso motions. Because the wavelet technique is less influenced by non-stationarity and the averaging time, it allows the study of the temporal evolution of detected structures and the possible identification of linear GWs.

The wavelet spectra (Eq. (6)) provide an estimation of the time evolution of the wavelet energy spectra of the analyzed signals at the different resolved time-scales. Figure 3 displays the wavelet spectra for the time series collected at 9 m in the submeso time-scale range. The increase of the wavelet energy density at 0130 LT highlights the activation of submeso structures with a characteristic time-scale of about 8 min until 0700 LT. In the first part of the night, the energy of the horizontal wind components reveals the presence of meandering motions that intensify their energy around 0300 LT. A similar behaviour is observed in the temperature and pressure fluctuation energy distribution. On the contrary, over the same time period the vertical wind velocity component does not show any activity at the same scales. The detected submeso structures are observed until 0630 LT with an energy activation of the vertical wind component at 0430 LT, characterized by the same time-scale of the other variables.

The wavelet spectra computed at 5 m (Figure S2) show a distribution of energy similar to that observed at 9 m for all the

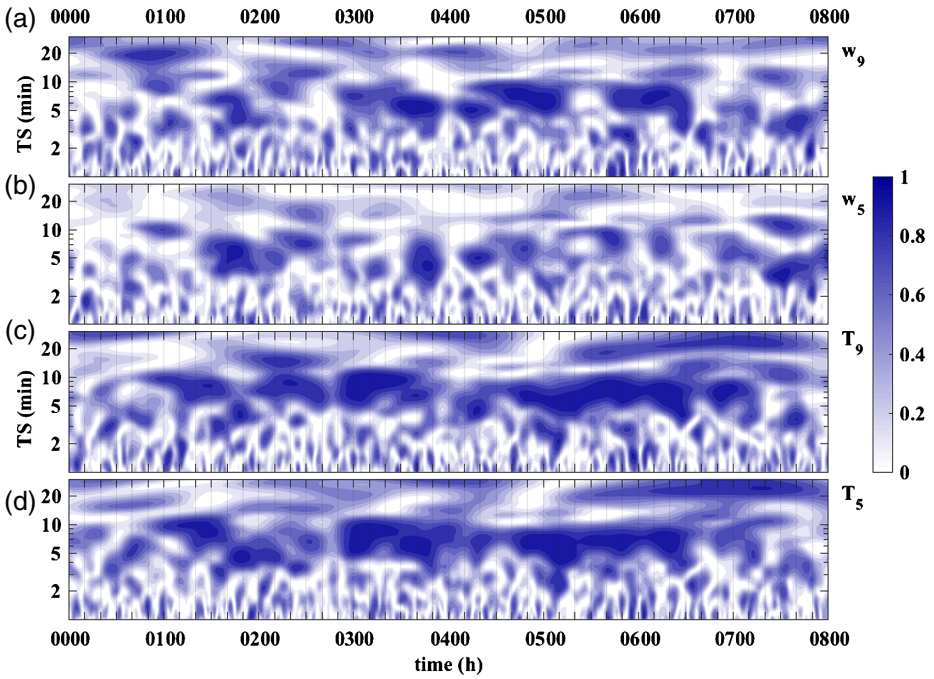

Figure 5. Time evolution in the submeso time-scale (TS) range of wavelet coherency spectra for the cross-correlation between pressure fluctuations and vertical wind component at (a) 9 m (w_9) and (b) 5 m (w_5) and temperature at (c) 9 m (T_9) and (d) 5 m (T_5) collected on 11 December 2007.

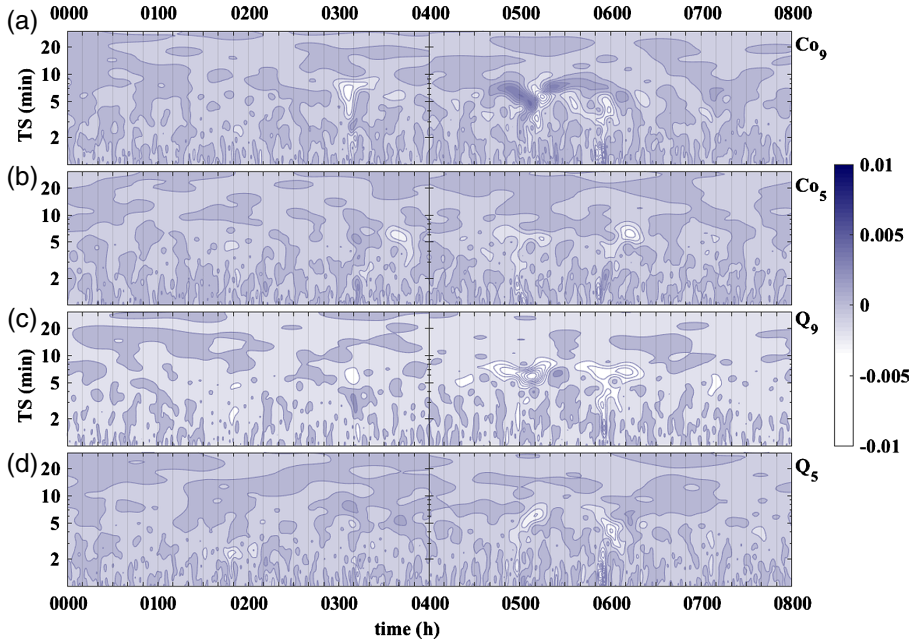

Figure 6. Time evolution in the submeso time-scale (TS) range of (a, b) wavelet cospectrum (Co) and (c,d) quadrature (Q) for the cross-correlation between the vertical wind component and the sonic temperature at (a, c) 9 m and (b,d) 5 m collected on 11 December 2007.

variables with the exception of w which does not present any submeso activity.

These results are in good agreement with the EAF analysis (Figure 2) and confirm the presence of meandering at a time-scale of the order of about 7 min.

The wavelet coherence spectra between the wind components and Δp show that the detected horizontal meandering (Figure 4) as well as the vertical oscillations (Figure 5) are highly correlated with pressure; in fact coherence spectra between Δp and horizontal components assume very high values ($Coh \approx 1$) after the activation of horizontal meandering (after 0100 LT in Figure 4) corresponding with the meandering time-scales. On the other hand, coherence spectrum between Δp and vertical component reaches maximum values after the activation of GWs at 9 m (after 0400 LT in Figure 5(a)).

Furthermore, the nature of detected vertical wave-like motions was analyzed through the wavelet cross-spectra between w and θ. The oscillating sign of the wavelet cospectrum and the high values of the quad-spectrum between 0430 and 0700 LT (Figure 6) highlight the lack of vertical diffusion (i.e. w and θ are 90° out of phase) and suggest the activation of linear GWs at 9 m, confirmed by the behaviour of wavelet coherence and phase spectra (Figure S3). The same analysis at 5 m displays an attenuation of the GWs probably because of the interaction with mechanical turbulence produced near the ground.

In order to investigate the influence of submeso motions on the turbulence production, the variances of the horizontal and vertical velocity components were split into submeso and turbulent contributions (Figure 7). On the basis of the hourly spectral behaviour (not shown), a clear and constant gap between the two kinds of motions was observed at a time-scale of about 4 min for the entire analysed period; hence, this value was chosen as the threshold to separate the wavelet coefficients. The submeso contribution was evaluated as the integral of the

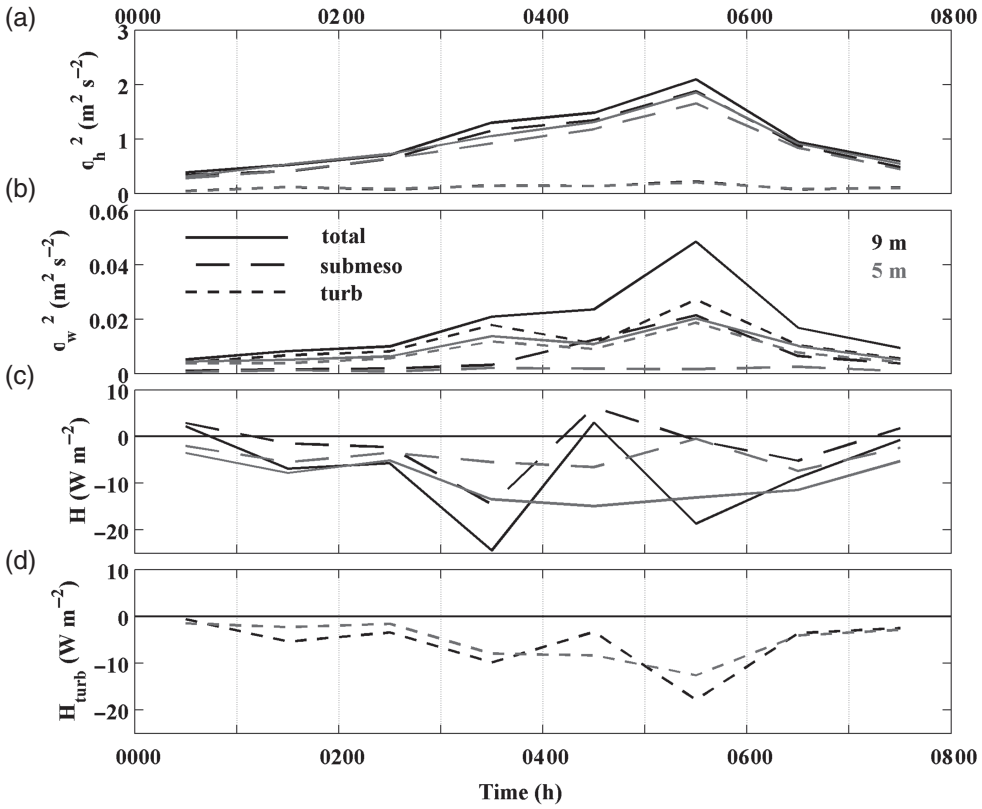

Figure 7. Mean variances of (a) horizontal and (b) vertical components and (c,d) sensible heat flux at 9 m (black lines) and 5 m (grey lines) on 11 December 2007. The total mean statistics (continuous lines) have been decomposed into submeso (long dashed lines: time-scale greater than 4 min) and turbulent contributions (short dotted lines: time-scale below 4 min). In order to highlight the erratic flux behaviour due to submeso scales, (c) mesoscale and (d) turbulent components have been shown separately.

wavelet coefficients relative to time-scales greater than 4 min, and the turbulent one as the integral of time-scales below 4 min. The total variance of horizontal velocity components is mainly due to the submeso contribution and the horizontal turbulent energy remains almost constant for the whole analysed period (Figure 7(a)). On the other hand, vertical turbulent energy increases simultaneously and exhibits the same magnitude of the submeso one at both levels (Figure 7(b)). This result can be explained by a mechanism of turbulent production in low-wind regimes by intermittent short-term wind accelerations above a height-dependent threshold value modulated by submeso motions, as suggested by Sun *et al.* (2012). It is also worth noticing that the ratio between the vertical and horizontal total standard deviations of the wind velocity (not shown) ranges between 0.10 and 0.15, well inside the prescribed values evaluated in Mortarini *et al.* (2016b) for the identification of meandering cases.

Finally, the same approach was applied for the separation of submeso and turbulent contributions to the vertical sensible heat flux (H, Figures 7(c) and (d)). The performed analysis shows that submeso motions (Figure 7(c)) can produce errors in both sign and magnitude of the computed fluxes and confirms the necessity of filtering the submeso scales for a correct estimation of the turbulent fluxes in stable conditions. In particular, Figure 7(c) shows as the activation of GWs (after 0400 LT at 9 m) can produce very small and/or counter-gradient fluxes, as already observed in other studies (Cava *et al.*, 2015; Sun *et al.*, 2015). The separation of the different motions highlights that the erratic flux behaviour is related to submeso scales (dashed lines in Figure 7(c)), in agreement with cross-spectral analysis shown in Figure 6. In fact the filtering of submeso motions corrects the turbulent H sign that remains negative after the activation of GWs (Figure 7(d)). Moreover, filtered turbulent heat flux intensifies after the intensification of submeso motions and, in particular, after the activation of GWs (after 0400 LT), since they can induce in the range of turbulent time-scales (TS < 4 min) a stronger intermittent turbulence production and a stronger vertical turbulent mixing than the horizontal meandering (Sun *et al.*, 2015).

5. Conclusions

In this article a night-time period of 8 h characterized by the coexistence of linear GWs and horizontal meandering was analysed with the aim of investigating the character of the two submeso phenomena simultaneously occurring in a low-wind-speed regime. Two different methods of analysis were applied to the three wind velocity components, the sonic temperature and the pressure fluctuations collected during the UTP campaign in Turin (Italy). The first method is based on the evaluation of the EAFs and it has been specifically implemented for meandering studies (Anfossi *et al.*, 2005). The second method is based on wavelet analysis, commonly used for GW detection and here applied to characterize the meandering motions. The two methodologies identified the same time-scale for the detected structures over the whole period. The wavelet analysis highlighted that, in this case, the horizontal meandering is not triggered by vertical GWs which were absent during the meandering activation and appeared later in the night.

The meandering phenomenon was observed with similar characteristics at both levels, while the GW presence was evident at 9 m but it appeared much weaker at 5 m, probably due to the interaction with mechanical turbulence produced near the ground. The cross-spectral wavelet analysis indicated high coherence between the pressure fluctuations and the horizontal components of the wind velocity, suggesting that the observed meandering was driven by pressure perturbations, as already pointed out by Mahrt (2007).

Both GWs and meandering contributed to an increase of the turbulent energy, especially in the vertical component of the wind velocity, in agreement with Sun *et al.* (2012). This behaviour confirmed the crucial role of submeso structures in the turbulence production during low-wind regimes in stable

conditions. Moreover, the correct determination of the turbulent fluxes required a proper filtering of the submeso components which may produce counter-gradient fluxes in particular when GWs are present.

Summarizing, the wavelet analysis proves to be a valuable tool for studying the activation and the evolution of horizontal meandering as a continuous function of time on different time-scales. Further, it allows the discrimination between the linear GWs and the pure horizontal meandering, which is often not feasible with the EAFs. The good agreement in the evaluation of the time-scales obtained with the two approaches confirmed how the EAFs and the loop parameter can be confidently used for the identification of the meandering cases, in particular in 'clean' cases when there is a clear separation between submeso and turbulent scales. However, the necessity to confirm and generalize the encouraging results obtained and to identify the limitations of the methodologies used requires their application to larger datasets collected in different conditions and experimental sites.

Supporting information

The following supporting information is available as part of the online article:

Figure S1. (a) EAFs for the u (black continuous lines) and v (black dashed lines) velocity components (top panel) and for the w velocity component (green dashed lines) and for the temperature θ (black continuous lines) (bottom panel) computed for the first four hours of the analysed period. The red lines represent the prescribed theoretical behaviour. (b) is as (a), but for the last four hours of the analysed period.

Figure S2. Time evolution in the submeso time-scale (TS) range of wavelet energy spectra of longitudinal (a), lateral (b) and vertical wind velocity components (c), temperature (d) collected at 5 m, and pressure fluctuations (e) collected at ground level on 11 December 2007.

Figure S3. Time evolution in the submeso time-scale (TS) range of wavelet coherency and phase spectra for the cross-correlation between temperature and vertical wind component at 9 m (Coh_9 and Φ_9, respectively) and at 5 m (Coh_5 and Φ_5, respectively) collected on 11 December 2007.

References

Anfossi D, Oettl D, Degrazia G, Goulart A. 2005. An analysis of sonic anemometer observations in low wind speed conditions. *Boundary-Layer Meteorol.* **114**: 179–203, doi: 10.1007/s10546-004-1984-4.

Anfossi D, Alessandrini S, Trini Castelli S, Ferrero E, Oettl D, Degrazia G. 2006. Tracer dispersion simulation in low wind speed conditions with a new 2D Langevin equation system. *Atmos. Environ.* **40**: 7234–7245, doi: 10.1016/j.atmosenv.2006.05.081.

Belušic D, Güttler I. 2010. Can mesoscale models reproduce meandering motions? *Q. J. R. Meteorol. Soc.* **136**: 553–565, doi: 10.1002/qj.606.

Belušić D, Mahrt L. 2008. Estimation of length scales from mesoscale networks. *Tellus A* **60**: 706–715, doi: 10.1111/j.1600-0870.2008.00328.x.

Cassardo C, Sacchetti D, Morselli MG, Anfossi D, Brusasca G, Longhetto A. 1995. A study of the assessment of air temperature, and sensible and latent heat fluxes from sonic anemometer observations. *Nuovo Cimento C* **18**: 419–440, doi: 10.1007/BF02511367.

Cava D, Giostra U, Tagliazucca M. 2001. Spectral maxima in a perturbed atmospheric boundary layer. *Boundary-Layer Meteorol.* **100**: 421–437, doi: 10.1023/A:1019219117439.

Cava D, Giostra U, Siqueira M, Katul GG. 2004. Organised motion and radiative perturbations in the nocturnal canopy sublayer above an even-aged pine forest. *Boundary-Layer Meteorol.* **112**: 129–157, doi: 10.1023/B:BOUN.0000020160.28184.a0.

Cava D, Schipa S, Giostra U. 2005. Investigation of low-frequency perturbations induced by a steep obstacle. *Boundary-Layer Meteorol.* **115**: 27–45, doi: 10.1007/s10546-004-2123-y.

Cava D, Giostra U, Katul G. 2015. Characteristics of gravity waves over an antarctic ice sheet during an austral summer. *Atmosphere* **6**: 1271–1289, doi: 10.3390/atmos6091271.

Chimonas G. 2002. On internal gravity waves associated with the stable boundary layer. *Boundary-Layer Meteorol.* **102**: 139–155, doi: 10.1023/A:1012730306799.

Daubechies I. 1992. *Ten Lectures on Wavelets*. CBMS-NSF Regional Conference Series in Applied Mathematics **61**. Society for Industrial and Applied Mathematics: Philadelphia, PA.

De Baas AF, Driedonks GM. 1985. Internal gravity waves in a stably stratified boundary layer. *Boundary-Layer Meteorol.* **31**: 303–323, doi: 10.1007/BF00120898.

Dias NL, Brutsaert W, Wesley ML. 1995. Z-less stratification under stable conditions. *Boundary-Layer Meteorol.* **75**: 175–187, doi: 10.1007/BF00721048.

Doran JC, Horst TW. 1981. Velocity and temperature oscillations in drainage winds. *J. Appl. Meteorol.* **20**: 360–364, doi: 10.1175/1520-0450(1981)020<0361:VATOID>2.0.CO;2.

Durden DJ, Nappo CJ, Leclerc MY, Duarte HF, Zhang G, Parker MJ, Kurzeja RJ. 2013. On the impact of wavelike disturbances on turbulent fluxes and turbulence statistics in nightime conditions: a case study. *Biogeosciences* **10**: 8433–8443, doi: 10.5194/bg-10-8433-2013.

Farge M. 1992. Wavelet transforms and their applications to turbulence. *Annu. Rev. Fluid Mech.* **24**: 395–457, doi: 10.1146/annurev.fl.24.010192.002143.

Frenkiel FN. 1953. Turbulent diffusion: mean concentration distribution in a flow field of homogeneous turbulence. *Adv. Appl. Mech.* **3**: 61–107, doi: 10.1016/S0065-2156(08)70208-4.

Goulart A, Degrazia G, Acevedo O, Anfossi D. 2007. Theoretical considerations of meandering wind in simplified conditions. *Boundary-Layer Meteorol.* **125**: 279–287, doi: 10.1007/s10546-007-9179-4.

Grinsted A, Moore JC, Jevrejeva S. 2004. Applications of the cross wavelet transform and wavelet coherence to geophysical time series. *Nonlin. Proc Geophys.* **11**: 561–566, doi: 10.5194/npg-11-561-2004.

Gupta S, McNider RT, Trainer M, Zamora RJ, Knupp K, Singh MP. 1997. Nocturnal wind structure and plume growth rates due to inertial oscillations. *J. Appl. Meteorol.* **36**: 1050–1063, doi: 10.1175/1520-0450(1997)036<1050:NWSAPG>2.0.CO;2.

Howell FJ, Mahrt L. 1997. Multiresolution flux decomposition. *Boundary-Layer Meteorol.* **83**: 117–137, doi: 10.1023/A:1000210427798.

Joffre S, Laurila T. 1988. Standard deviations of wind speed and direction from observations over a smooth surface. *J. Appl. Meteorol.* **27**: 550–561, doi: 10.1175/1520-0450(1988)027<0550:SDOWSA>2.0.CO;2.

Katul G, Vidakovic B. 1998. Identification of low-dimensional energy containing flux transporting eddy motion in the atmospheric surface layer using wavelet thresholding methods. *J. Atmos. Sci.* **55**: 377–389, doi: 10.1175/1520-0469(1998)055<0377:IOLDEC>2.0.CO;2.

Kumar P, Foufoula-Georgiou E. 1997. Wavelet analysis for geophysical applications. *Rev. Geophys.* **35**: 385–412, doi: 10.1029/97RG00427.

Luhar A. 2012. Lagrangian particle modelling of dispersion in light winds. In *Lagrangian Modeling of the Atmosphere*, AGU Geophysical Monograph 200, Lin JC, Brunner D, Gerbig C, Stohl A, Luhar A, Webley P. (eds.): 37–51. American Geophysical Union: Washington, DC.

McMillen RT. 1988. An eddy correlation technique with extended applicability to non-simple terrain. *Boundary-Layer Meteorol.* **43**: 231–245, doi: 10.1007/BF00128405.

Mahrt L. 1999. Stratified atmospheric boundary layers. *Boundary-Layer Meteorol.* **9**: 375–396, doi: 10.1023/A:1001765727956.

Mahrt L. 2007. Weak-wind mesoscale meandering in the nocturnal boundary layer. *Environ. Fluid Mech.* **7**: 331–347, doi: 10.1007/s10652-007-9024-9.

Mahrt L. 2010. Variability and maintenance of turbulence in the very stable boundary layer. *Boundary-Layer Meteorol.* **135**: 1–18, doi: 10.1007/s10546-009-9463-6.

Mahrt L. 2011. The near-calm stable boundary layer. *Boundary-Layer Meteorol.* **140**: 343–360, doi: 10.1007/s10546-011-9616-2.

Mahrt L. 2014. Stably stratified atmospheric boundary layers. *Annu. Rev. Fluid Mech.* **46**: 23–45, doi: 10.1146/annurev-fluid-010313-141354.

Mahrt L, Mills R. 2009. Horizontal diffusion by submeso motions in the stable boundary layer. *Environ. Fluid Mech.* **9**: 443–456, doi: 10.1007/s10652-009-9126-7.

Mortarini L, Ferrero E, Falabino S, Trini Castelli S, Richiardone R, Anfossi D. 2013. Low-frequency processes and turbulence structure in a perturbed boundary layer. *Q. J. R. Meteorol. Soc.* **139**: 1059–1072, doi: 10.1002/qj.2015.

Mortarini L, Maldaner S, Moor L, Stefanello M, Acevedo O, Degrazia G, Anfossi D. 2016a. Temperature auto-correlation and spectra functions in low-wind meandering conditions. *Q. J. R. Meteorol. Soc.* **142**: 1881–1889, doi: 10.1002/qj.2796.

Mortarini L, Stefanello M, Degrazia G, Roberti D, Trini Castelli S, Anfossi D. 2016b. Characterization of wind meandering in low-wind-speed conditions. *Boundary-Layer Meteorol.* **161**: 165–182, doi: 10.1007/s10546-016-0165-6.

Murgatroyd RJ. 1969. Estimations from geostrophic trajectories of horizontal diffusivity in the mid-latitude troposphere and lower stratosphere. *Q. J. R. Meteorol. Soc.* **95**: 40–62, doi: 10.1002/qj.49709540304.

Nappo CJ. 2002. *An Introduction to Atmospheric Gravity Waves*. Academic Press: New York, NY.

Nappo CJ, Sun J, Mahrt L, Belušić D. 2014. Determining wave–turbulence interactions in the stable boundary layer. *Bull. Am. Meteorol. Soc.* **95**: ES11–ES13, doi: 10.1175/BAMS-D-12-00235.1.

Nieuwstadt FTM. 1984. The turbulent structure of the stable, nocturnal boundary layer. *J. Atmos. Sci.* **41**: 2202–2216, doi: 10.1175/1520-0469(1984)041<2202:TTSOTS>2.0.CO;2.

Oettl D, Almbauer RR, Sturm PJ. 2001. A new method to estimate diffusion in stable, low-wind conditions. *J. Appl. Meteorol.* **40**: 259–268, doi: 10.1175/1520-0450(2001)040<0259:ANMTED>2.0.CO;2.

Oettl D, Goulart A, Degrazia G, Anfossi D. 2005. A new hypothesis on meandering atmospheric flows in low wind speed conditions. *Atmos. Environ.* **39**: 1739–1748, doi: 10.1016/j.atmosenv.2004.11.034.

Rees JM, Denholm-Price JCW, King JC, Anderson PS. 2000. A climatological study of internal gravity waves in the atmospheric boundary layer. *J. Atmos. Sci.* **57**: 511–526, doi: 10.1175/1520-0469(2000)057<0511:ACSOIG>2.0.CO;2.

Rees JM, Staszewski WJ, Winkler JR. 2001. Case study of a wave event in the stable atmospheric boundary layer overlying an Antarctic ice shelf using orthonormal wavelet transform. *Dyn. Atmos. Oceans* **34**: 245–261, doi: 10.1016/S0377-0265(01)00070-7.

Richiardone R. 1993. The transfer function of a differential microbarometer. *J. Atmos. Oceanic Tech.* **10**: 624–628, doi: 10.1175/1520-0426(1993)010<0624:TTFOAD>2.0.CO;2.

Sharan M, Modani M, Yadav A. 2003. Atmospheric dispersion: an overview of mathematical modeling framework. *Proc. Indian Natl. Sci. Acad. A* **69**: 725–744.

Sorbjan Z, Czerwinska A. 2013. Statistics of turbulence in the stable boundary layer affected by gravity waves. *Boundary-Layer Meteorol.* **148**: 73–91, doi: 10.1007/s10546-013-9809-y.

Steeneveld GJ, Holtslag AAM. 2011. Meteorological aspects of air quality. In *Air Quality in the 21st Century*, Romano GC, Conti AG. (eds.): 67–114. Nova Science: New York, NY.

Sun J, Lenschow DH, Burns SP, Banta RM, Newsom RK, Coulter R, Frasier S, Ince T, Nappo C, Balsley B, Jensen M, Mahrt L, Miller D, Skelly B. 2004. Atmospheric disturbances that generate intermittent turbulence in nocturnal boundary layers. *Boundary-Layer Meteorol.* **110**: 255–279, doi: 10.1023/A:1026097926169.

Sun J, Mahrt L, Banta RM, Pichugina YL. 2012. Turbulence regimes and turbulence intermittency in the stable boundary layer during CASES-99. *J. Atmos. Sci.* **69**: 338–351, doi: 10.1175/JAS-D-11-082.1.

Sun J, Mahrt L, Nappo C, Lenschow DH. 2015. Wind and temperature oscillations generated by wave-turbulence interactions in the stably stratified boundary layer. *J. Atmos. Sci.* **72**: 1484–1503, doi: 10.1175/JAS-D-14-0129.1.

Terradellas E, Soler M, Ferreres E, Bravo M. 2005. Analysis of oscillations in the stable boundary layer using wavelet methods. *Boundary-Layer Meteorol.* **114**: 489–518, doi: 10.1007/s10546-004-1293-y.

Thomas C, Foken T. 2005. Detection of long- term coherent exchange over spruce forest using wavelet analysis. *Theor. Appl. Climatol.* **80**: 91–104, doi: 10.1007/s00704-004-0093-0.

Torrence C, Compo GP. 1998. A practical guide to wavelet analysis. *Bull. Am. Meteorol. Soc.* **79**: 61–78, doi: 10.1175/1520-0477(1998)079<0061:APGTWA>2.0.CO;2.

Trini Castelli S, Falabino S, Mortarini L, Ferrero E, Richiardone R, Anfossi D. 2014. Experimental investigation of the surface layer parameters in low-wind conditions in a suburban area. *Q. J. R. Meteorol. Soc.* **140**: 2023–2036, doi: 10.1002/qj.2271.

Vercauteren N, Mahrt L, Klein R. 2016. Investigation of interactions between scales of motion in the stable boundary layer. *Q. J. R. Meteorol. Soc.* **142**: 2424–2433, doi: 10.1002/qj.2835.

Viana S, Terradellas S, Yague C. 2010. Analysis of gravity waves generated at the top of a drainage flow. *J. Atmos. Sci.* **67**: 3949–3966, doi: 10.1175/2010JAS3508.1.

Vickers D, Mahrt L, Belušić D. 2008. Particle simulations of dispersion using observed meandering and turbulence. *Acta Geophys.* **56**: 234–256, doi: 10.2478/s11600-007-0041-3.

Wyngaard JC. 2010. *Turbulence in the Atmosphere*. Cambridge University Press: Cambridge, UK.

